Nanoscale Res Lett (2008) 3:454–460
DOI 10.1007/s11671-008-9180-y

NANO EXPRESS

Thermodynamic Properties of Supported and Embedded Metallic Nanocrystals: Gold on/in SiO_2

F. Ruffino · M. G. Grimaldi · F. Giannazzo · F. Roccaforte · V. Raineri

Received: 17 July 2008 / Accepted: 17 September 2008 / Published online: 9 October 2008

Abstract We report on the calculations of the cohesive energy, melting temperature and vacancy formation energy for Au nanocrystals with different size supported on and embedded in SiO_2. The calculations are performed crossing our previous data on the surface free energy of the supported and embedded nanocrystals with the theoretical surface-area-difference model developed by W. H. Qi for the description of the size-dependent thermodynamics properties of low-dimensional solid-state systems. Such calculations are employed as a function of the nanocrystals size and surface energy. For nanocrystals supported on SiO_2, as results of the calculations, we obtain, for a fixed nanocrystal size, an almost constant cohesive energy, melting temperature and vacancy formation energy as a function of their surface energy; instead, for those embedded in SiO_2, they decreases when the nanocrystal surface free energy increases. Furthermore, the cohesive energy, melting temperature and vacancy formation energy increase when the nanocrystal size increases: for the nanocrystals on SiO_2, they tend to the values of the bulk Au; for the nanocrystals in SiO_2 in correspondence to sufficiently small values of their surface energy, they are greater than the bulk values. In the case of the melting temperature, this phenomenon corresponds to the experimentally well-known superheating process.

Keywords Nanocrystal · Surface energy · Gold · SiO_2 · Cohesive energy · Melting temperature · Vacancy formation energy

F. Ruffino (✉) · M. G. Grimaldi
Dipartimento di Fisica e Astronomia, Università di Catania, via S. Sofia 64, I-95123 Catania, Italy
e-mail: francesco.ruffino@ct.infn.it

F. Ruffino · M. G. Grimaldi
MATIS CNR-INFM, Catania, Italy

F. Giannazzo · F. Roccaforte · V. Raineri
Consiglio Nazionale delle Ricerche—Istituto per la Microelettronica e Microsistemi (CNR-IMM) Stradale Primosole 50, I-95121 Catania, Italy

Introduction

The physical and chemical properties of low-dimensional solid-state systems draw considerable attention, in the previous years, because of their technological importance [1, 2]. In particular, the properties of nanocrystals (NCs) differ from that of the corresponding bulk materials, mainly due to the additional energetic term of $\gamma_0 A$, i.e. the product of the surface excess free energy γ_0 and the surface area A. This term becomes significant to change the physical and chemical properties of the NCs (with respect to the bulk material) due to the large surface/volume ratio of such systems. So, the properties of NCs bridge those of bulk materials and atomic scale systems [3]. Also, the thermodynamic properties of NCs are different from that of the corresponding bulk materials and the study of such properties acquired a fundamental relevance in the last decades [4–34] because of their applications in the field of microelectronics, solar energy utilization and nonlinear optics. For example, nowhere is the interest in the thermodynamics of materials at small dimensions than in the microelectronics industry, where transistors and metal interconnects will have tolerances of only several nanometres [35]. One particular phenomenon of interest is, for example, the size-dependent melting point of NCs with respect to the corresponding bulk materials [4–11]: this phenomenon received considerable attention since Takagi in 1954 experimentally

demonstrated that ultrafine metallic NCs melt below their corresponding melting temperature [4]. It is now known that the melting temperature of all low-dimensional solid-state systems (NCs, nanowires and nanosheets), including metallic [5–8], organic [9, 10] and semiconductor [11] depends on their size. For free standing NCs, the melting temperature decreases as its size decreases, while for NCs supported on or embedded in a matrix, they can melt below or above the melting point of the corresponding bulk crystal depending on the interface structure between the NCs and the surrounding environment (the substrate or the matrix) [12–18]. If the interfaces are coherent or semi-coherent, an enhancement of the melting point is present: this phenomenon is called superheating [12–14, 16, 18]. Otherwise, there is a depression of the melting point [16–18]. Not only the melting temperature but also several thermodynamic parameters, such as cohesive energy (the energy needed to divide the crystal into isolated atoms) and vacancy formation energy (the energy to form a vacancy in the NC in thermodynamic equilibrium) of NCs have been the subject of several experimental [19] and theoretical [18, 20–28] studies. Several methods have been developed and used to measure the thermodynamic properties of nanosystems (nanocalorimetry [17], scanning probe microscopy [29, 30], transmission electron microscopy [31], X-ray diffraction [32]) and different models were developed to describe the size-dependent thermodynamic properties of such systems (BOLS model [20], latent heat model [21], liquid drop model [18], surface-area-difference (SAD) model [22, 23], bond energy [24]). So, the importance of the combination of experimental and theoretical works towards a complete understanding of the thermodynamic properties of free-standing, supported and embedded nano-systems is clear.

In a previous experimental work [33], we fabricated supported/embedded Au NCs on/in SiO_2. Using high-resolution transmission electron microscopy (HR-TEM) and by the inverse Wulff construction, we were able to obtain the angular-dependent surface energy $\gamma_0(\theta)$ of the supported and embedded NCs as a function of their size. The main result of that work was that growing NCs surrounded by an 'isotropic' environment (Au in SiO_2) exhibit an angular and radial symmetrical surface free energy function $\gamma_0(\theta)$ making the surface stress tensor f_{ij} of the NC rotationally and translationally invariant: this situation determines a symmetrical equilibrium shape of the NCs. Growing NCs in a 'non-isotropic' environment (Au on SiO_2) exhibit a surface energy $\gamma_0(\theta)$, that lost its angular and radial symmetry for sufficiently large sizes, determining the loss of the rotational and translational invariance of the f_{ij} and, as a consequence, a loss of symmetry in the equilibrium shape of the NC and the formation of internal defects.

In the present paper, we cross our experimental data concerning the surface free energy of the Au NCs supported on SiO_2 and embedded in SiO_2 with the SAD theoretical model of Qi [23] for the description of the size-dependent thermodynamic properties of metallic NCs, to simulate (and so to predict) the cohesive energy, the melting temperature and the vacancy formation energy for the Au NCs supported on and embedded in SiO_2. In particular, we compare such quantities for Au NCs with the same size but supported or embedded on/in the SiO_2 layer finding significant differences derived from the different effects of the surrounding environment. We believe that our theoretical results can improve the understanding of the thermodynamic properties of NCs and can guide future experimental investigations.

Experiment and results

Cz- $<100>$ silicon substrates (with resistivity $\rho \approx 6 \times 10^{-3}$ Ω cm) were etched in a 10% aqueous HF solution to remove the native oxide, and subsequently annealed at 1,223 K for 15 min in O_2 in order to grow an uniform, 10 nm thick, amorphous SiO_2 layer. A 2-nm thick Au film was deposited (at room temperature) by sputtering on the SiO_2 layer using an Emitech K550x Sputter coater apparatus (Ar plasma, 10^{-4} Pa pressure). In some samples, the Au layer was covered by a 3-nm thick SiO_2 layer deposited (at room temperature) by sputtering using an AJA RF Magnetron sputtering apparatus (Ar plasma, 1.3×10^{-8} Pa pressure). Then, the Au/SiO_2 and SiO_2/Au/SiO_2 samples were contemporary annealed in Ar ambient in the 873–1073 K temperature range and in the 5–60 min time range to obtain the growth of NCs [33, 34].

The samples were analyzed by HR-TEM (after mechanical polishing and final Ar ion milling) using a Jeol 2010F energy-filtered transmission microscope (EF-TEM), operating at 200 kV and equipped with a Gatan image filtering apparatus. Before the cross-sectional TEM analyses of the samples with Au on SiO_2, a thin SiO_2 cap-layer ($\sim$3 nm) was deposited (by sputtering with the AJA RF Magnetron apparatus) on the samples in order to protect the NCs during the samples preparation.

From the HR-TEM images of the Au NCs embedded in SiO_2, with diameter in the range 2 nm $< D <$ 7 nm it is clear that they conserve an equilibrium shape symmetry (single icosahedral crystal) increasing the size [33, 34].

Differently, the Au NCs growing on SiO_2, belong to three different groups on the basis of their equilibrium shape and internal atomic structure, as a function of their diameter D (in the range 2 nm $< D <$ 7 nm for our case):

group 1: formed by NCs with a diameter $D < 3$ nm. They have a structure such as the Au NCs in SiO_2, i.e. single icosahedral crystal;

group 2: formed by NCs with a diameter 3 nm < D < 4 nm. They have an icosahedral structure characterized by twins of the (111) atomic planes;
group 3: formed by the NCs with a radius 4 nm < D < 14 nm. They have a complicated decahedral multitwinned (and lamellar) structure.

We extracted quantitative information on the surface free energy from these NCs shape via the inverse Wulff construction [33] that gives the dependence of the step free energy on the orientation starting from the NC equilibrium shape. In fact, it is possible to construct the inverse of the free energy as the minimal surface of the Wulff-construction to the shape of $1/r(\theta)$: first, we identified the 'Wulff point' of the NC as the intersection point between the perpendicular bisectors of two {111} facets. This point was taken as the centre of a polar plot, with angular and radial coordinates θ and r. For each given ray projecting from the origin of the polar plot in the angle θ_i (measured with a 5° spacing), we searched for the perpendicular which is a tangent to the equilibrium shape. Then we measured the distance r_i between the Wulff point and this tangent. According to the Wulff relation $\gamma_0(\theta_i)/r(\theta_i) = \lambda = \text{const}$, the value of the surface free energy for the NCs $\gamma_0(\theta_i)$ for those orientation was obtained and the $\gamma_0(\theta)$ plot was determined. The results shown in Fig. 1 were the obtained $\gamma_0(\theta_i)$, and are reported as normalized to the surface free energy of the (111) plane of the Au (1.363 J/m^2, [18]). Figure 1a shows the obtained $\gamma_0(\theta)$ (each averaged on 10 NCs) for NCs on SiO_2 for different average NCs diameter: black for a NC on SiO_2 with mean diameter of 2.5 nm, red with mean diameter of 3.5 nm and green of 7 nm. Figure 1b shows $\gamma_0(\theta)$ (each averaged on 10 NCs) for NCs in SiO_2 with the same mean size: black for a mean diameter of 2.5 nm, red with mean diameter of 3.5 nm and green of 7 nm. The NC-to-NC variation in $\gamma_0(\theta)$ for a given orientation is indicated as the error bars for some points. Form Fig. 1b, it is clear that growing NCs in SiO_2 maintain the angular dependence of their surface energy unchanged. Instead, from Fig. 1a, it is clear that growing NCs on SiO_2 undergo an evident modification of their surface free energy. The differences in $\gamma_0(\theta)$ for NCs with same diameter but supported and embedded in SiO_2 are explained in terms of the angular and radial symmetry/asymmetry of the NC surface free energy corresponding to a symmetrical/asymmetrical spatial situation of the environment surrounding the NC correlated with the rotational/translational invariance of the surface stress tensor f_{ij} of the NC [33]. In particular, in the continuation of the present work, we are interested in the $\gamma_0(\theta_i)$ values reported in Fig. 1. In fact, crossing such values with the theoretical model of Qi [23] for the description of the size-dependent thermodynamic properties of NCs, we are able to predict

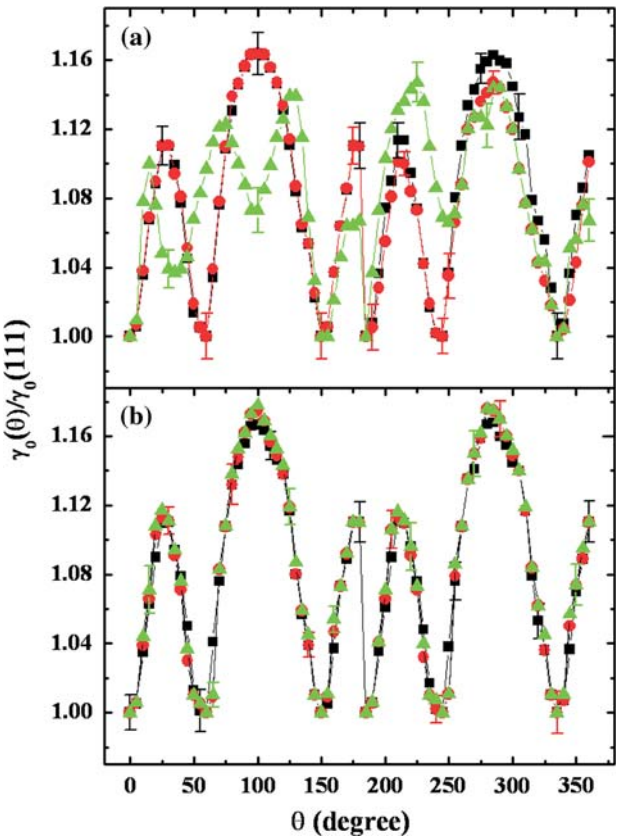

Fig. 1 (a) Experimental Wulff plot ($\gamma_0(\theta)$) for the Au NCs on SiO_2: black, red and green points refer to NC with diameter of D = 2.5, 3.5, 7 nm, respectively; (b) Experimental Wulff plot ($\gamma_0(\theta)$) for the Au NCs in SiO_2: black, red and green points refer to NC with diameter of D = 2.5, 3.5, 7 nm, respectively

the cohesive energy, melting temperature and vacancy formation energy for the Au NCs supported and embedded on/in SiO_2. First to continue, a comparison between our results on the surface energy of supported/embedded Au NCs with respect to the work of Nanda et al. [36] on the surface energy of free Ag nanoparticles is meaningful: they investigated the size-dependent evaporation of free Ag nanoparticles by online heat treatment of size-classified aerosols at different temperatures for a particular time period. The linear relation between the evaporation temperature and the inverse of the particle size verifies the Kelvin effect, and from the slope, a constant value of 7.2 J/m^2 is obtained for the surface energy of free Ag nanoparticles, higher than that of the bulk one (1.065–1.54 J/m^2). The work of Nanda was performed on 'free' Ag nanoparticles of diameter ~14–16 nm and, for such a system, a constant value of surface energy between 5 and 6 times higher than the bulk value was inferred. In our case, the Au nanoparticles have a diameter in the range of 1–14 nm and they are supported on a substrate (SiO_2) or embedded in a matrix (SiO_2). And, as recognized also by

Nanda, the nanoparticle–surrounding environment interaction strongly affects the surface energy value. As expected, also for the Au nanoparticles supported or embedded on/in SiO_2 a higher value of the surface energy with respect to the bulk one was evaluated, but only between 1 and 1.18 times higher (see Fig. 1). In particular, for the same size, higher values were found for the nanoparticles embedded in SiO_2 (1–1.18 times higher than the bulk value, Fig. 1b) with respect to the nanoparticles supported on SiO_2 (1–1.16 times higher than the bulk value, Fig. 1a).

Theoretical model, simulations and discussion

Qi et al. [23] developed a SAD model to describe the thermodynamic properties of metallic NCs and several experimental confirmations of the model were presented [23]. This model is based on the knowledge of the surface (or interface) free energy of the NC to simulate size-dependent thermodynamic properties of the NC such as cohesive energy, melting temperature and vacancy energy formation.

The cohesive energy is an important physical quantity that accounts for the bond strength of a solid, which equals the energy needed to divide the solid into isolated atoms by breaking all the bonds. It is also a fundamental quantity in determining other important thermodynamic properties such as the melting temperature of the solid and the vacancy formation energy [37]. The cohesive energy of a bulk crystal is constant at a given temperature [38], because of the small surface to volume ratio. But this ratio becomes significant in low-dimensional systems such as NCs. The experimental size-dependence of the cohesive energy for low-dimensional systems for Mo and W NCs was reported for the first time in 2002 [19], while the size-dependence of the melting temperature has been known already for a long time [4, 5]. Also, the vacancy formation energy is size-dependent in low-dimensional systems [23]. Vacancies are very important defects in materials, and have a remarkable effect on the physics of materials, such as electrical resistance and heat capacity. Therefore, the importance of knowing its dependence on the NCs size is clear.

The SAD model developed by Qi et al. [23] describes the size-dependent cohesive energy, melting temperature and vacancy energy formation for low-dimensional systems in an excellent way. Therefore, our aim is to implement such a model with our experimental data on the surface free energy of supported and embedded Au NCs on/in SiO_2 to simulate (i.e. to predict) their cohesive energy, melting temperature and vacancy formation energy as a function of the surface free energy and size. To this aim, we recall briefly the results of the model, whose extensive description can be found in [23].

We name E_{cB}, T_{mB}, E_{vB} the cohesive energy, the melting temperature and the vacancy formation energy, respectively, of the bulk solid. E_{cNC}, T_{mNC}, E_{vNC} those of the NC (0-dimensional system), which depend on the diameter D by the formulas:

$$E_{cNC} = E_{cB}\left(1 - \frac{3p\alpha d_{hkl}}{D}\right) \quad (1)$$

$$T_{mNC} = T_{mB}\left(1 - \frac{3p\alpha d_{hkl}}{D}\right) \quad (2)$$

$$E_{vNC} = E_{vB}\left(1 - \frac{3p\alpha d_{hkl}}{D}\right) \quad (3)$$

In these formulas, we have $p = \gamma_i/\gamma_0$ and $\gamma_i = \gamma_0 - q\gamma_M$. γ_0 is the surface free energy of the crystal per unit area (J/m^2) at 0 K. γ_i is the interface energy (per unit area) between the crystal and the surrounding matrix [18, 23]. γ_M is the surface energy (per unit area) of the surrounding matrix at 0 K. $0 \leq q \leq 1$ is a parameter that describes the coherence between the crystal and the matrix [18]. $q = 1$ describes the case of a completely coherent interface, $q = 0.5$ a semi-coherent interface, $q = 0$ the non-coherent interface (is the same as that of the crystal with the free surface). The parameter α is a shape factor: it accounts for the shape difference between spherical and non-spherical NCs [18, 23, 26, 27]. It is defined as the ratio of surface area between non-spherical and spherical NCs in an identical volume. For spherical NCs, $a = 1$. d_{hkl} is the interplanar distance of (hkl).

Equations 1–3 with the appropriate values of γ_0, γ_M, q, α, d_{hkl} describe very well the size-dependent cohesive energy, melting temperature and vacancy formation energy of NCs and they are used to predict such thermodynamic quantities for several low-dimensional solid-state systems [23].

We use Eqs. 1–3 in this work in connection with the experimental data on the surface free energy of Au NCs on and in SiO_2 (Fig. 1) to simulate E_{cNC}, T_{mNC}, E_{vNC} as a function of $\gamma_0(\theta_i)$ and D for the supported and embedded NCs.

For the simulation routines, we fix in Eqs. 1–3 three different NCs sizes: $D = 2.5$, 3.5, 7 nm both for the Au NCs on and in SiO_2. γ_M is fixed as the value of the surface free energy of SiO_2: $\gamma_M(SiO_2) = 1.5\ J/m^2$ [39, 40]. The shape factor α for regular polyhedral NCs ranges from 1 to 1.49 [23], so that for the present calculations the mean value of 1.245 is chosen. d_{hkl} is computed for a cubic crystal (Au has a FCC structure) as $d_{hkl} = a/\sqrt{h^2 + k^2 + l^2}$ with α as the Au lattice parameter. It is known that the

surface energy of small index of the surface plane may be lower than that of the large index of the surface plane, and as a result the surface with small index may have low total energy, which means that the crystal with the small index plane may be more stable. This is surely true for the Au NCs on and in SiO_2 that are surrounded by {100} crystal planes. Therefore, in these cases we fix, for the calculations $d_{100} = 0.40788$ nm [41]. It is known that the Au NCs on SiO_2 are of a strong non-wetting nature, with a very high contact angle [42]; therefore the Au/SiO_2 interface is surely a very small fraction of the entire Au surface. As a consequence, for the specific calculations, we assume $q = 0.1$ for the case of Au NCs on SiO_2, while for the case of Au in SiO_2, we assume $q = 1$(coherent interface). Finally, about the Au bulk values we fix: $E_{cB} = 3.81$ eV [38], $T_{mB} = 1337.34$ K [5], $E_{vB} = 0.97$ eV/at [43]. Using these values, and the Eqs. 1–3, for each values of $\gamma_O(\theta_i)$ the resulting values of E_{cNC}, T_{mNC}, E_{vNC} were obtained for the Au NCs on and in SiO_2 for the fixed values of sizes. The results are reported in Figs. 2–4 for the cohesive energy, melting temperature and vacancy formation energy, respectively.

Figure 2 reports the results for the cohesive energy simulations: black, red and green points indicate the calculations for the cohesive energy, as a function of the surface free energy $\gamma_O(\theta)$, for Au NCs supported on SiO_2 with diameter of $D = 2.5$ nm, $D = 3.5$ nm, $D = 7$ nm,

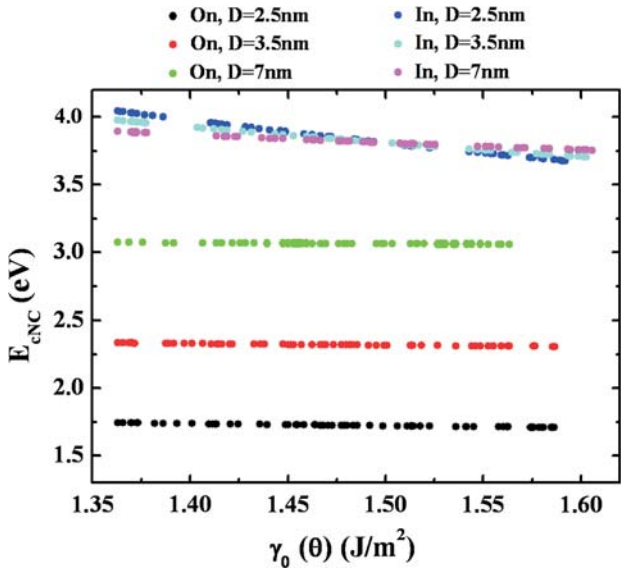

Fig. 2 Black, red and green points refer to the calculated values of the cohesive energy (as a function of $\gamma_0(\theta)$) for Au NCs on SiO_2 with diameter of $D = 2.5$, 3.5, 7 nm, respectively. Blue, cyan and magenta points refer to the calculated values of the cohesive energy (as a function of $\gamma_0(\theta)$) for Au NCs in SiO_2 with diameter of $D = 2.5$, 3.5, 7 nm, respectively. The calculations are performed using $\gamma_M(SiO_2) = 1.5$ J/m^2, $\alpha = 1.245$, $d_{100} = 0.40788$ nm, $q = 0.1$ for the Au NCs on SiO_2 and $q = 1$ for the Au NCs in SiO_2

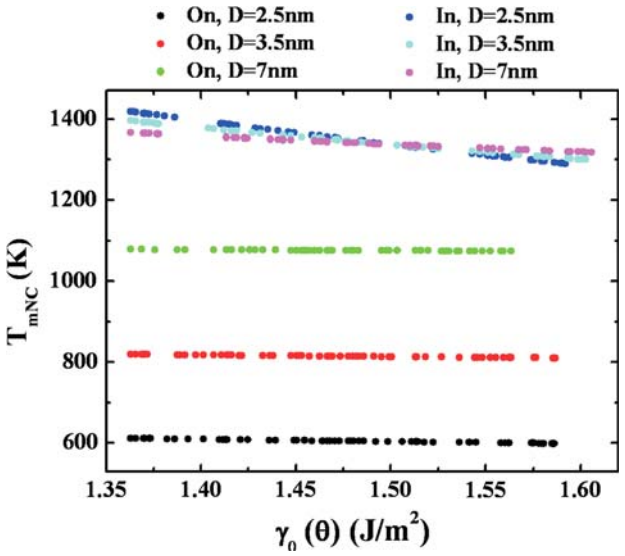

Fig. 3 Black, red and green points refer to the calculated values of the melting temperature (as a function of $\gamma_0(\theta)$) for Au NCs on SiO_2 with diameter of $D = 2.5$, 3.5, 7 nm, respectively. Blue, cyan and magenta points refer to the calculated values of the melting temperature (as a function of $\gamma_0(\theta)$) for Au NCs in SiO_2 with diameter of $D = 2.5$, 3.5, 7 nm, respectively. The calculations are performed using $\gamma_M(SiO_2) = 1.5$ J/m^2, $\alpha = 1.245$, $d_{100} = 0.40788$ nm, $q = 0.1$ for the Au NCs on SiO_2 and $q = 1$ for the Au NCs in SiO_2

respectively; blue, cyan and magenta points indicate the calculated values for Au NCs embedded in SiO_2 with diameter of $D = 2.5$, 3.5, 7 nm, respectively.

Figure 3 reports the results for the melting temperature simulations: black, red and green points indicate the calculations for the melting temperature, as a function of the surface free energy $\gamma_O(\theta)$, for Au NCs supported on SiO_2 with diameter of $D = 2.5$, 3.5, 7 nm, respectively; blue, cyan and magenta points indicate the calculated values for Au NCs embedded in SiO_2 with diameter of $D = 2.5$, 3.5, 7 nm, respectively.

Figure 4 reports the results for the vacancy formation energy simulations: black, red and green points indicate the calculations for the vacancy formation energy, as a function of the surface free energy $\gamma_O(\theta)$, for Au NCs supported on SiO_2 with diameter of $D = 2.5$, 3.5, 7 nm, respectively; blue, cyan and magenta points indicate the calculated values for Au NCs embedded in SiO_2 with diameter of $D = 2.5$, 3.5, 7 nm, respectively. Our calculations predict higher cohesive energy, melting temperature and vacancy formation energy, at equal sizes, for the Au NCs embedded in SiO_2 with respect to those supported on SiO_2. Furthermore, while the cohesive energy, melting temperature and vacancy formation energy are almost constant for the Au NCs on SiO_2 (the value increases by increasing the NCs size, tending to the melting temperature of the bulk Au) as a function of $\gamma_O(\theta)$, they show a slightly decrease for the Au

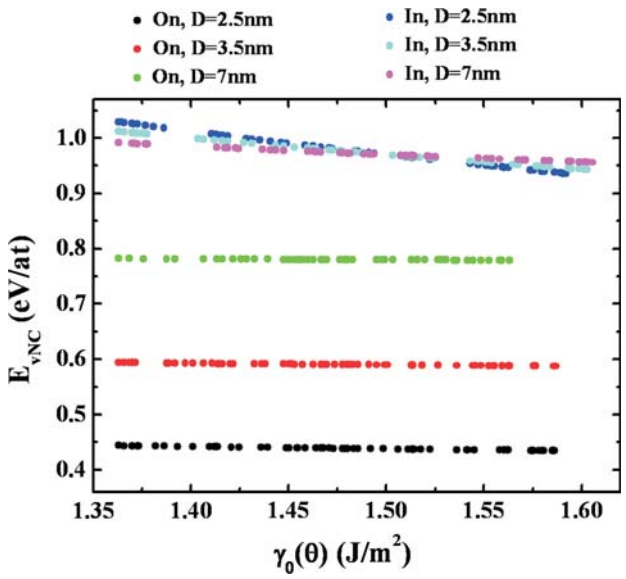

Fig. 4 Black, red and green points refer to the calculated values of the vacancy formation energy (as a function of $\gamma_0(\theta)$) for Au NCs on SiO_2 with diameter of $D = 2.5$, 3.5, 7 nm, respectively. Blue, cyan and magenta points refer to the calculated values of the vacancy formation energy (as a function of $\gamma_0(\theta)$) for Au NCs in SiO_2 with diameter of $D = 2.5$, 3.5, 7 nm, respectively. The calculations are performed using $\gamma_M(SiO_2) = 1.5$ J/m^2, $\alpha = 1.245$, $d_{100} = 0.40788$ nm, $q = 0.1$ for the Au NCs on SiO_2 and $q = 1$ for the Au NCs in SiO_2

in SiO_2. Furthermore, it is worth to observe that for the smaller Au NCs embedded in SiO_2 exist a range of $\gamma_0(\theta)$ values for which E_{cNC}, T_{mNC}, E_{vNC} assume values greater than that of the respective bulk values. This phenomenon is due to the coherent interface between the NCs and the matrix. In the case of the melting temperature, this phenomenon is known as superheating and it is experimentally verified for some embedded small metallic NCs [12–14, 16, 18]. In addiction, our calculations show that the cohesive energy, melting temperature and vacancy formation energy for embedded NCs, not only depend on NCs size D on the index $\{hkl\}$ of the interface plane, but also on the direction θ by the direction dependent interface energy $\gamma_0(\theta)$. This means that, for example, embedded NCs melt preferentially along specific directions (i.e. specific crystal planes) or, also, that it is easier to generate vacancy in the NCs along specific atomic planes with respect to the other planes. This phenomena characterize embedded NCs but not support NCs with the same size.

Conclusion

In this paper, we reported the calculations of the cohesive energy, melting temperature and vacancy formation energy for Au NCs supported on SiO_2 and embedded in SiO_2 for different diameters ($D = 2.5$, 3.5, 7 nm) as a function of the NCs surface (interface) free energy. The calculations were performed by implementing our experimental data concerning the surface (interface) free energy $\gamma_0(\theta)$ in the SAD model developed by Qi et al. for the description of the size-dependent thermodynamic properties of low-dimensional solid-state systems. Some differences in the thermodynamic behaviour of Au NCs supported and embedded on/in SiO_2 are found:

(1) For the Au NCs on SiO_2, the cohesive energy, melting temperature and vacancy formation energy are almost constant with $\gamma_0(\theta)$;
(2) The constant values of the cohesive energy, melting temperature and vacancy formation energy for the Au NCs on SiO_2 increase when the NCs size increases, tending to the values of the bulk Au;
(3) For the Au NCs in SiO_2, the cohesive energy, melting temperature and vacancy formation energy decrease when $\gamma_0(\theta)$ increases;
(4) The constant values of the cohesive energy, melting temperature and vacancy formation energy for the Au NCs in SiO_2 increase when the NCs size increases;
(5) For the smaller NCs in SiO_2, in correspondence of opportune small values of $\gamma_0(\theta)$, the values of the cohesive energy, melting temperature and vacancy formation energy are greater than the bulk values.

References

1. *Nanoparticles and Nanostructured Films Preparation, Characterization and Applications*, ed. by J. H. Fendler (Wiley, Weinheim, 1998)
2. *Nanoparticles*, ed. by G. Schmid (Wiley, Weinheim, 2004)
3. R.L. Johnston, *Atomic and Molecular Clusters* (Taylor and Francis, London, 2002)
4. M. Takagi, J. Phys. Soc. Jpn. **9**, 359 (1954). doi:10.1143/JPSJ.9.359
5. P.A. Buffat, J.P. Borel, Phys. Rev. A **13**, 2287 (1976). doi:10.1103/PhysRevA.13.2287
6. M. Hasegawa, K. Hoshino, M. Watanabe, J. Phys. F Metab. Phys. **10**, 619 (1980). doi:10.1088/0305-4608/10/4/013
7. Q. Jiang, H.Y. Tong, D.T. Hsu, K. Okuyama, F.G. Shi, Thin Solid Films **312**, 357 (1998). doi:10.1016/S0040-6090(97)00732-3
8. Q. Jiang, N. Aya, F.G. Shi, Appl. Phys. A **64**, 627 (1997). doi:10.1007/s003390050529
9. Q. Jiang, H.X. Shi, M. Zhao, J. Chem. Phys. **111**, 2176 (1999). doi:10.1063/1.479489
10. K. Morishige, K. Kawano, J. Phys. Chem. B **103**, 7906 (1999). doi:10.1021/jp991177m
11. A.N. Goldstein, Appl Phys. A **62**, 33 (1996). doi:10.1007/BF01568084
12. K. Chattopadhyay, R. Goswami, Prog. Mater. Sci. **42**, 287 (1993). doi:10.1016/S0079-6425(97)00030-3
13. D.L. Zhang, B. Cantor, Acta Metall. Mater. **39**, 1595 (1991). doi:10.1016/0956-7151(91)90247-X
14. R. Goswami, K. Chattopadhyay, Philos. Mag. Lett. **68**, 215 (1993). doi:10.1080/09500839308242415

15. N.B. Thoft, J. Bohr, B. Buras, E. Johnson, A. Johansen, J. Phys. D: Appl Phys (Berl) **28**, 539 (1995)
16. H. Sheng, G. Ren, L.M. Peng, Z.Q. Hu, K. Lu, J. Mater. Res. **12**, 119 (1997). doi:10.1557/JMR.1997.0019
17. M. Zhang, M.Y. Efremov, F. Schiettekatte, E.A. Olson, A.T. Kwan, S.L. Lai, T. Wisleder, J.E. Greene, L.H. Allen, Phys. Rev. B **62**, 10548 (2000). doi:10.1103/PhysRevB.62.10548
18. K.K. Nanda, S.N. Sahu, S.N. Behera, Phys. Rev. A **66**, 013208 (2002). doi:10.1103/PhysRevA.66.013208
19. H.K. Kim, S.H. Huh, J.W. Park, J.W. Jeong, G.H. Lee, Chem. Phys. Lett. **354**, 165 (2002). doi:10.1016/S0009-2614(02)00146-X
20. C.Q. Sun, Y. Wang, B.K. Tay, S. Li, H. Huang, Y. Zhang, J. Phys. Chem. B **106**, 10701 (2002). doi:10.1021/jp025868l
21. Q. Jiang, J.C. Li, B.Q. Chi, Chem. Phys. Lett. **366**, 551 (2002). doi:10.1016/S0009-2614(02)01641-X
22. W.H. Qi, M.P. Wang, J. Mater. Sci. Lett. **21**, 1743 (2002). doi:10.1023/A:1020904317133
23. W.H. Qi, M.P. Wang, M. Zhou, W.Y. Hu, J. Phys. D: Appl. Phys. (Berl) **38**, 1429 (2005)
24. W.H. Qi, M.P. Wang, M. Zhou, G.Y. Xu, Chem. Phys. Lett. **372**, 632 (2003). doi:10.1016/S0009-2614(03)00470-6
25. W.H. Qi, M.P. Wang, Physica B **334**, 432 (2003). doi:10.1016/S0921-4526(03)00168-6
26. W.H. Qi, M.P. Wang, Mater. Chem. Phys. **88**, 280 (2004). doi:10.1016/j.matchemphys.2004.04.026
27. W.H. Qi, Solid State Commun. **137**, 536 (2006). doi:10.1016/j.ssc.2006.01.018
28. W.H. Qi, Physica B **368**, 46 (2005). doi:10.1016/j.physb.2005.06.035
29. M. Dippel, A. Maier, V. Gimple, H. Wider, W.E. Evenson, R.L. Rasera, G. Schatz, Phys. Rev. Lett. **87**, 095505 (2001). doi:10.1103/PhysRevLett.87.095505
30. G. Krausch, T. Detzel, H.N. Biefeled, R. Fink, B. Luckscheiter, R. Platzer, U. Wöhormann, G. Schatz, Appl. Phys. A **53**, 324 (1991). doi:10.1007/BF00357195
31. R. Goswami, K. Chattopadhyay, P.L. Ryder, Acta Mater. **46**, 4257 (1998). doi:10.1016/S1359-6454(98)00094-9
32. K.F. Peters, J.B. Cohen, Y.-W. Chung, Phys. Rev. B **57**, 13430 (1998). doi:10.1103/PhysRevB.57.13430
33. F. Ruffino, M.G. Grimaldi, C. Bongiorno, F. Giannazzo, F. Roccaforte, V. Raineri, Nanoscale Res. Lett. **2**, 240 (2007). doi:10.1007/s11671-007-9058-4
34. F. Ruffino, M.G. Grimaldi, C. Bongiorno, F. Giannazzo, F. Roccaforte, V. Raineri, Superlattices Microstruct. (2008) (in press). doi:10.1016/j.spmi.2008.01.001
35. K.K. Likharev, Electronics below 10 nm, in *Nano and Giga Challenges in Microelectronics*, ed. by J. Greer, et al. (Elsevier, Amsterdam, 2003), pp. 27–68
36. K.K. Nanda, A. Maisels, F.E. Kruis, H. Fissan, S. Stappert, Phys. Rev. Lett. **91**, 106102 (2003). doi:10.1103/PhysRevLett.91.106102
37. J.H. Rose, J. Ferrante, J.R. Smith, Phys. Rev. Lett. **47**, 675 (1981). doi:10.1103/PhysRevLett.47.675
38. C. Kittel, *Introduction to Solid State Physics*, 7th edn. (Wiley, New York, 1996)
39. Q. Jiang, H.M. Lu, M. Zhao, J. Phys. Condens. Matter **16**, 521 (2004). doi:10.1088/0953-8984/16/4/001
40. Y.K. Shchipalov, Glass Ceram. **57**, 374 (2000). doi:10.1023/A:1010900903019
41. C.S. Barrett, T.B. Massalski, *Structure of Metals*, 3rd revised edn. (Oxford, Pergamon, 1980)
42. F. Ruffino, A. Canino, M.G. Grimaldi, F. Giannazzo, C. Bongiorno, F. Roccaforte, V. Raineri, J. Appl. Phys. **101**, 064306 (2007). doi:10.1063/1.2711151
43. W. Triftshäuser, J.D. McGervey, Appl. Phys. A **6**, 177 (1975)